Consiglio Nazionale delle Ricerche

Istituto per i Polimeri, Compositi e Biomateriali - UOS di Napoli/Portici

PROGRAMMA DI RICERCA STM

Research Report

Development of advanced polymeric materials based on the use of biopolymers, ionic liquids and graphene for high-barrier packaging applications.

Guest researcher: Ricardo Keitel Donato

Host: Giovanna G. Buonocore

May, 2015

1 Introduction

Biodegradable polymers e.g., vinyl alcohol resins (PVOH), are becoming strong competitors for conventional non-degradable polymer resins for high performance packaging,[1] biomedical applications[2] and membrane separation.[3] However, their generally inferior barrier and thermo-mechanical properties allow only specific functions and short-term packaging films production.[4] The physical and/or chemical modifications of PVOH have been studied in order to obtain new functional materials applied in more broad range of fields.[5] Chemical crosslinking,[6,7] filling[3,8,9] or grafting[10] are some of common techniques used for material properties enhancement. The PVOH's elevated hydrogen bonding (H-bond) capacity, high chain flexibility and excellent water solubility opens a great field for incorporating fillers or additives which can use these characteristics for morphology and interphase tuning. Our group has been studying the effects of ionic liquids (IL) as compatibilizers and properties enhancers in various polymeric systems.[11-14] Ionic liquids (IL) are biodegradable organic salts with ionic-covalent crystalline structures which keep the liquid state at temperatures below 100 °C.[15] These multifunctional surfactants present high thermal and chemical resistance, stability in air and moisture as well as insignificant flammability and volatility.[16] Previously reported studies mostly discuss the use of IL in order to improve electrical, electrochemical or thermal properties of PVOH,[17-19] not exploring their potential as multifunctional surfactants in nanocomposites PVOH systems.

The production and use of graphene became of strategic interest, representing a promise of breakthroughs for several areas, especially materials sciences. The biggest challenges for obtaining and using graphene are the low efficiency of the available methods, which the mostly commonly used involves an aggressive oxidation, creating dispersed graphene oxide (GO) sheets or ribbons (Hummer method).[20] The search for milder conditions and higher graphene yields led to several procedures, among which the irradiation of carbon species dispersions in solvents and/or surfactants presented significant results.[11-23] The imidazolium-based IL present these properties together with the strong capacity of interacting with carbon based materials. A "π-π stacking" of the IL cations at the π-electronic surface of the sp^2 carbon network allows it to act as both solvent and surfactant due to the IL's amphiphilic structure.[24] These features make IL ideal for exfoliating/stabilizing graphene through a solution irradiation process,

allowing broader experimental conditions, as soon as volatile organic solvents have the drawback of limited working temperature ranges.

In the present report we evaluate the effects of different IL (Fig. 1) in a PVOH derivative (G-Polymer™), as well as the application of graphene into the same systems. Thus, we can observe both the effect of graphene in the presence of G-polymer and the IL effect in the polymer-filler interphase. Samples were prepared by solvent casting and investigated as for their structural, morphological, thermo-mechanical and barrier properties.

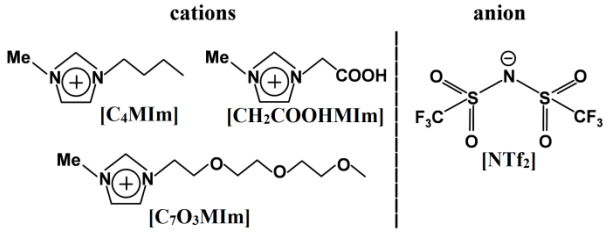

Fig. 1 The alkyl [C_4MIm][NTf_2], carboxyl [CH_2COOHMIm][NTf_2] and ether-functionalized [C_7O_3MIm][NTf_2] IL applied in this work.

2 Experimental

2.1 Materials

The Nichigo G-Polymer™ grade: OKS8049 (GP) glassy, low crystalline, low foaming, transparent, amorphous vinyl alcohol resin was purchased from NIPPON GOHSEI, Japan. Three classes of imidazolium IL were used. The alkyl-IL 1-butyl-3-methylimidazolium bis(trifluoromethylsulfonyl)imide [C_4MIm][NTf_2] was purchased from IoLiTec Ionic Liquids Technologies Inc. A procedure reported previously in the literature was used for the synthesis of the ether-IL 1-triethylene glycol monomethyl ether-3-methylimidazolium methanesulfonate [C_7O_3MIm][MeS],[25] which was used as precursor for the preparation of the IL 1-triethylene glycol monomethyl ether-3-methylimidazolium bis(trifluoromethylsulfonyl)amide [C_7O_3MIm][NTf_2]. The [C_7O_3MIm][NTf_2] was prepared by anion exchange using [C_7O_3MIm][MeS] and lithium bis(trifluoromethylsulfonyl)amide ($LiNTf_2$) in 1:1 proportion. Salts were stirred for 2 days in dichloromethane, obtained LiMeS was filtrated and [C_7O_3MIm][NTf_2] dried using vacuum pump. The purity of IL was evaluated by ^{1}H NMR, where spectral data of the [C_7O_3MIm][MeS] was in the accordance with the literature,[25] and the disappearance the of [MeS] characteristic peak was observed for the [C_7O_3MIm][NTf_2] (**Fig. 2**). Also for the carboxylic-IL 1-methyl-3-methylcarboxylic acid imidazolium

bis(trifluoromethylsulfonyl)imide [$CH_2COOHMIm$][NTf_2], a previously published method was applied.[26] Before application, IL were dried under vacuum for 5h at 60 °C. Bi-distilled water was purchased from Best-Chemical s.r.l. For the first experiments a synthetic graphite (Timrex SFG6, Timcal primary synthetic graphite) was used. Due to the short term of this tryout, only the results for synthetic graphite will presented in this report, but samples with natural graphite, with longer lamellae range, were produced and results will be further characterized.

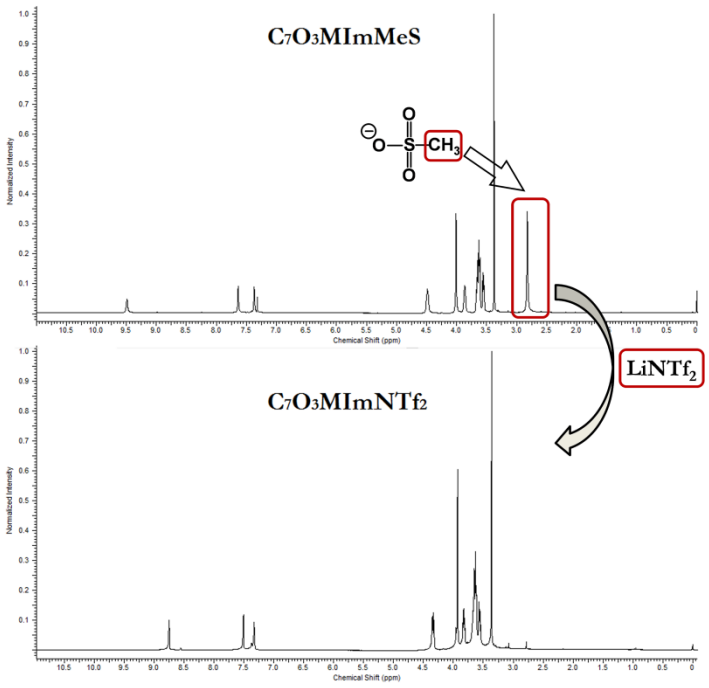

Fig. 2 ^{1}H-NMR spectra of the anion exchange process from [C_7O_3MIm][MeS] to [C_7O_3MIm][NTf_2]

2.2 Preparation of GP-IL and GP-IL-graphene films

Initially, a 10% solution of GP was prepared by adding it (2.40 g) into the water (21.60 g) and stirring until homogenous (~2h at 60 °C). The IL was added into the cooled GP solution, stirred for 5 min, applied 10 min to an ultrasound bath and poured into a Petri dish. For the samples with graphite, it was added to the GP-IL-water solution, applied for 10 min to an ultrasound bath for graphite spreading and further applied for a another ultrasound machine (Hielscher UP200S working at 200 W, f = 24 kHz) for graphite homogenization, and eventually delamination, for 1h. The GP-IL-water solution and the homogeneous GP-IL-graphene water suspensions were left to cast at room temperature for 48 h and then dried under vacuum (8h at 60 °C). Before analysis films were thermal treated above glass transition temperature (T_g) for 1h at 120

°C under vacuum. For reader's clearer understanding, short-hand notations were used for GP-IL-graphene. The abbreviations (e.g. GP-C_4MImNTf_2) were used for samples modified with corresponding IL.

2.3 Films characterization

Differential Scanning Calorimetry: The TA Instruments DSC Q1000 calibrated with indium standards was used for analyses. Entire thermal scan was conducted under a nitrogen atmosphere with gas flow rate of 50 mL/min. Each sample had initial weight ~10 mg and was placed in a closed aluminum specimen holder before placing it in the oven. In order to erase thermal history of the samples, preliminary heating cycle was applied at rate of 20 °C/min. The measurements were made in the first cooling scan and in the second heating scan, where samples were heated and cooled at rate of 10 °C/min from 0 °C to 240 °C. The change of melting (ΔH_m), as well as crystallization (ΔH_c) enthalpies were obtained from integrated the area under endothermic or exothermic peak of the DSC thermogram, respectively. The maximum of the endothermic melting peak was considered as melting temperature (T_m) and similarly, the crystallization temperature (T_c) was taken as the maximum of the exothermic peak. The glass transition temperature (T_g) was obtained from the melting curve at transition's midpoint.

Thermogravimetric Analyses: Thermogravimetric analyses (TGA) were carried out at a heating rate of 10 °C/min from 40 °C to 800 °C using TA Instruments QA-500 or QA-5000. All experiments were conducted under air (QA-500) or nitrogen (QA-5000) atmosphere with gas flow rate of 60 or 25 mL/min, respectively. Sample (~10.0 mg) was placed in platinum crucible and an empty platinum pan was used as reference for all measurements. The residue (left at 700 °C), temperature of highest degradation rate (T_d), as well as temperatures at 5%, 10% and 50% of weight loss ($T_{5\%}$, $T_{10\%}$ and $T_{50\%}$) were determined. The T_d relates to the maximum temperature peak of first TGA derivative curve (DTG). The ashes from both procedures were collected.

Water vapor barrier properties: The measurements of water vapour permeability were performed using the infrared sensor technique by means of a PermatranW3/31 (Mocon, Germany). Samples with a surface area of 5 cm^2 were tested at 23 °C.

Dynamic Mechanical Analyses: A TA model QA 800 instrument was used for dynamic mechanical analyses (DMA) of the materials at a fixed frequency of 1 Hz and strain amplitude of 0.05%. DMA analyses were performed in the tensile mode, and the

rectangular specimens were heated from 30 °C to 130 °C at a rate of 3 °C/min. Before analysis, samples were conditioned at 30 °C for 24h. The DMA measurements were performed in triplicate.

3 Results and discussion

Thin GP hybrid films were prepared in the presence of the three different IL (**Fig. 1**). All the IL presented the same anion, as we previously characterized it as the most suitable for interacting with carbon nanospecies.[14] In this first tryout we are focusing in the differences of the applied IL in the process, independent of the efficiency of the graphite delamination. Further experiments, with the IL detected as the most suitable, will optimize the process. All obtained thin films were homogenous and transparent. The films with graphite application presented a reflective light gray tone, suggesting the absence of large clusters in the graphite dispersion.

3.1 Thermal behavior

The GP hybrids were studied by DSC and TGA analysis in order to estimate how graphite and IL affected thermal transitions, as well as thermal degradation. **Figure 3** shows the semi-crystalline polymer characteristic curves with both exothermic and endothermic events obtained by the DSC. In comparison with the pure GP matrix, the T_g of all modified samples increased confirming the direct filler-interaction with polymer matrix. Results with and without IL increase the T_g values (**Tab. 1**). This is a consequence of the decrease in the molecular mobility of polymer chains, suggesting that applying this content of IL it works as compatibilizer rather than plasticizer.

Table 1 Thermal transition profiles of hybrids.

Sample	T_g [a] [°C]	T_m [a] [°C]	T_c [a] [°C]
GP	66.1	184.3	156.4
GP-graphene	73.7	184.8	135.1
GP-C_4MImNTf_2-graphene	73.2	184.9	147.9
GP-COOHMImNTf_2-graphene	73.7	185.1	146.1
GP-C_7O_3MImNTf_2-graphene	73.2	185.6	148.8

[a] obtained from DSC measurements

For all samples the T_m remained practically unaltered, while the T_c is significant shifted to lower temperatures, representing the delay of crystallization caused by the presence of graphite (-20 °C, **Fig. 3a vs. b**). The application of any of the LI seem to

decrease this effect in about 10 °C, which could be an indication of nucleation effect of the IL on the graphite surface.

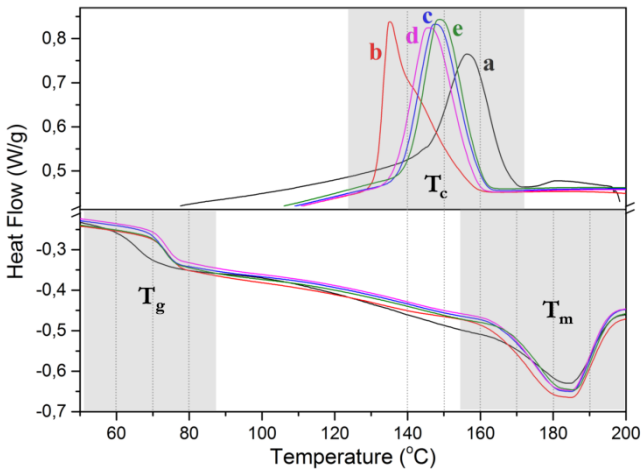

Fig. 3 Crystallization (T_c), glass transition (T_g) and melting (T_m) temperatures of (a) GP; (b) GP-graphite; (c) GP-C_4MImNTf$_2$; (d) GP-CH_2COOHMImNTf$_2$; (e) C_7O_3MImNTf$_2$.

Figure 4 shows the TGA and DTG curves for all samples at both inert (N_2) and oxidative (synthetic air) atmospheres. Under nitrogen atmosphere, pure GP shows 4 degradation stages which are related to its complex structure. Only the initial thermal resistance improved for samples with graphite and IL, where apparently the dominant contribution is from the filler (**Fig. 4a**). For samples measured under oxidative atmosphere, no significate difference could be observed among them.

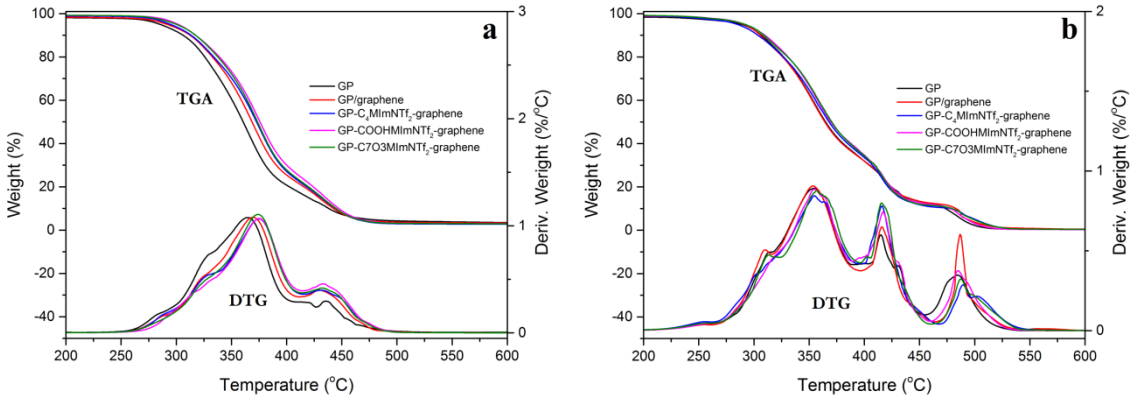

Fig. 4 Representative TGA and DTG curves of GP, GP-graphite, GP-C_4MImNTf$_2$-graphene, GP-COOHMImNTf$_2$-graphene and GP-C_7O_3MImNTf$_2$-graphene.

3.3 Mechanical properties

The DMA measurements were performed to observe the filler reinforcement in the GP matrix. **Figure 5** presents the storage modulus and the tan delta values for all

hybrids. Only the hybrid with the aliphatic chain IL (GP-C_4MImNTf_2) presented higher modulus than the neat GP, while the ones with polar groups in the cation showed a decrease in modulus (**Fig. 5(1)**). This could indicate that the polar groups are interacting with GP in a way that disrupts its organization, while the aliphatic one could form well spread isolated IL-graphite domains, which will be further evaluated by SAXS and WAXS. The tan delta curves showed the T_g values of all the hybrids we smaller than the neat GP, also showing some level of plasticization (**Fig. 5(2)**). Interestingly, these values do not correspond directly with the ones obtained by DSC, suggesting the hybrids are sensible to strain induced phenomena.

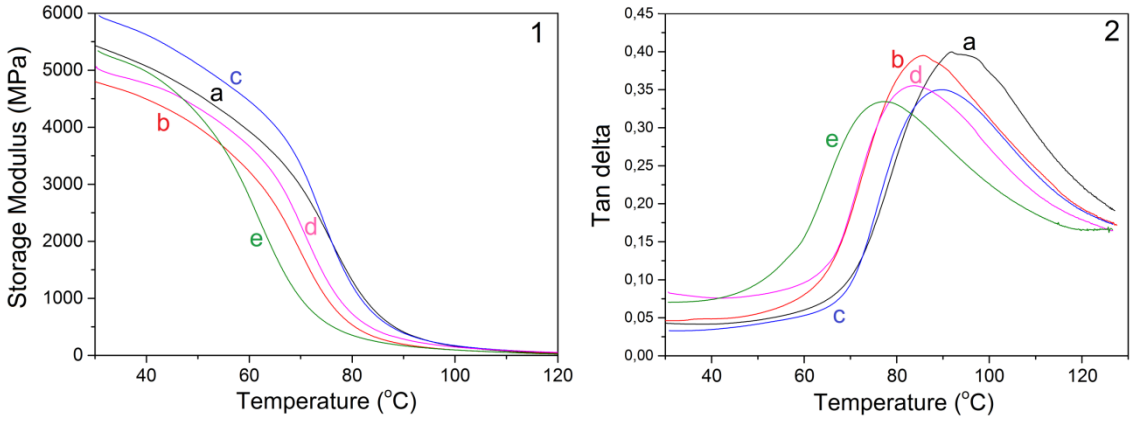

Fig. 5 Representative DMA curves showing storage modulus (1) and Tan delta (2) of (a) GP; (b) GP-graphite; (c) GP-C_4MImNTf_2; (d) GP-CH_2COOHMImNTf_2; (e) C_7O_3MImNTf_2.

3.5 Water vapor permeation

As graphite is a hydrophobic lamellar filler, the water vapor barrier properties of the hybrids were measured via water vapor permeation test. All the hybrids present higher water vapor permeation profile than neat GP (**Fig. 6**). This could be for the same reasons as the ones presented for the thermal and mechanical profiles, where the original structure of GP is affected by the graphite addition. The GP is a polymer with natural high barrier properties, which can be disrupted by addition of fillers, if not in a highly efficient manner. The hybrids GP-graphite, GP-C_7O_3MImNTf_2 and GP-CH_2COOHMImNTf_2 presented the highest increase in permeation, indicating that the IL with polar groups affect less efficiently the graphite dispersion. The GP-C_4MImNTf_2 presents a more mild permeation increase, presenting a profile more similar to neat GP. Two main reasons could be attributed to that; (i) higher graphite dispersion efficiency and/or (ii) formation of more hydrophobic domains by the IL aliphatic chains, decreasing the water diffusion.

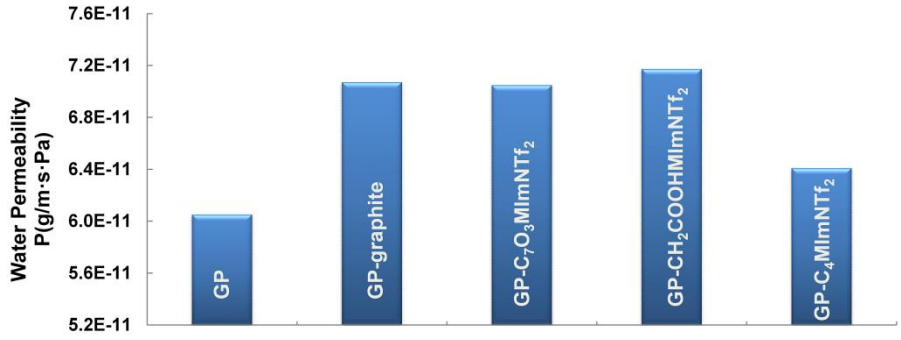

Fig. 6 Water vapor permeation profiles of GP and GP-graphite hydrids.

4 Conclusions

The use of IL to improve the graphite dispersion into GP and the reflexes of this dispersion into the GP properties were evaluated. The initial results show a relatively low dispersion efficiency, causing a negative reflex in the thermal and mechanical properties of the GP. Apparently, the IL with polar groups exerted a smaller influence in both graphite dispersion and GP properties, while $C_4MImNTf_2$ decreased the negative influences. This reinforces previous observations that amphiphilicity has a key role in graphite dispersion and delamination. Furthermore, the polar groups seem to interfere in the GP original packing, affecting the barrier and mechanical properties, while $C_4MImNTf_2$ allows a less disruptive procedure. In the next research steps, the influences of IL with different aliphatic chain functionalized cation will be studied for understanding better the role of the amphipaticity in the graphite delamination process. Also, the used of graphite with larger lamellae and the process parameters will be evaluated, followed by morphological characterizations, for improving the GP properties.

5 References

1. A. Musetti, K. Paderni, P. Fabbri, A. Pulvirenti, M. Al-Moghazy, P. Fava *J. Food Sci.* 2014, 79, E577.

2. M.I. Baker, S.P. Walsh, Z. Schwartz, B.D. Boyan *J Biomed Mater Res Part B* 2012, 100B, 1451.

3. S.J. Lue, D.-T. Lee, J.-Y. Chen, C.-H. Chiu, C.-C. Hu, Y.C. Jean, J.-Y. Lai *J. Membr. Sci.* 2008, 325, 831.

4. G. Bang, S.W. Kim, *J. Ind. Eng. Chem.* 2012, 18, 1063.
5. E. Marin, J. Rojas, Y. Ciro Afr. *J. Pharm. Pharmacol.* 2014, 8, 674.
6. M. Krumova, D. Lopez, R. Benavente, C. Mijangos, J.M. Perenã *Polymer* 2000, 41, 9265.
7. A. Hasimi, A. Stavropoulou, K.G. Papadokostaki, M. Sanopoulou Eur. *Polym.* J. 2008, 44, 4098.
8. S.-D. Jiang, Z.-M. Bai, G. Tang, Y. Hu , L. Song *Compos. Sci. Tech.* 2014, 102, 51.
9. Q.G. Zhang, Q.L. Liu, F.F., Y. Xiong *J. Mater. Chem.* 2008, 18, 4646.
10. N. Alghezawi, O. Sanlı, L. Aras and G. Asman, *Chem. Eng. Process.* 2005, 44, 51.
11. R.K. Donato, M.A. Benvegnú, L.G. Furlan, R.S. Mauler, H.S. Schrekker, *J. Appl. Polym. Sci.* 2010, 116, 304.
12. R.K. Donato, K.Z. Donato, H.S. Schrekker, L. Matějka, *J. Mater. Chem.* 2012, 22, 9939.
13. R.K. Donato, L. Matějka, H.S. Schrekker, J. Pleštil, A. Jigounov, J. Brus, M. Šlouf, *J. Mater. Chem.* 2011, 21, 13801.
14. A.C. Kleinschmidt, R.K. Donato, M. Perchacz, H. Beneš, V. Štengl, S.C. Amico, H.S. Schrekker *RSC Adv.* 2014, 4, 43436.
15. D. Coleman, N. Gathergood *Chem. Soc. Rev.* 2010, 39, 600.
16. P. Wasserscheid, T. Welton, Ionic Liquids in Synthesis, Wiley-VCH Verlag GmbH & Co. KGaA, Weinheim (2008).
17. A.L. Saroj, R.K. Singh *J. Phys. Chem. Solids* 2012, 73, 162.
18. Y. Zhang, R. Yan, F. Zhao, B. Zeng *Colloids Surf. B* 2009, 71, 288.
19. C.-W. Liew, S. Ramesh, A.K. Arof Inter. J. Hydrogen Energ. 2014, 39, 2953.
20. W.S. Hummers, R.E. Offerman *J. Am. Chem. Soc.* 1958, 80, 1339.
21. L. Jiao, X. Wang, G. Diankov, H. Wang, H. Dai, *Nat. Nanotechnol.* 2010, 5, 321.
22. Y. Hernandez, V. Nicolasi, M. Lotya *et al Nat. Nanotechnol.* 2008, 3, 563.
23. A.A. Green, M.C. Hersam *Nano Lett.* 2009, 9, 4031.
24. T. Fukushima, T. Aida *Chem. Eur. J.* 2007, 13, 5048.
25. H.S. Schrekker, D.O. Silva, M.A. Gelesky, M.P. Stracke, C.M.L. Schrekker, R.S. Gonçalves and J. Dupont *J. Braz. Chem. Soc.* 2008, 19, 426.
26. Z. Fei, D. Zhao, T.J. Geldbach, R. Scopelliti, P.J. Dyson *Chem. Eur. J.* 2004, 10, 4886.